

Binding potentials and interaction gates between microwave-dressed Rydberg atoms

David Petrosyan^{1,2} and Klaus Mølmer³

¹*Aarhus Institute of Advanced Studies, Aarhus University, DK-8000 Aarhus C, Denmark*

²*Institute of Electronic Structure and Laser, FORTH, GR-71110 Heraklion, Crete, Greece*

³*Department of Physics and Astronomy, Aarhus University, DK-8000 Aarhus C, Denmark*

(Dated: December 3, 2024)

We demonstrate finite range binding potentials between pairs of Rydberg atoms interacting with each other via attractive and repulsive van der Waals potentials and driven by a microwave field. We show that, using destructive quantum interference to cancel single-atom Rydberg excitation, the Rydberg-dimer states can be selectively and coherently populated from the two-atom ground state. This can be used to realize a two-qubit interaction gate which is not susceptible to mechanical forces between the atoms and is therefore immune to motional decoherence.

PACS numbers: 32.80.Ee, 32.80.Rm, 32.80.Qk 03.67.Lx,

Atoms in high-lying Rydberg states exhibit a number of remarkable features, including long lifetimes and giant polarizability [1]. The resulting strong, long-range, resonant (Förster) and nonresonant (van der Waals) dipole-dipole interactions between the atoms can suppress multiple Rydberg excitations within a certain blockade distance [2–5]. In combination with laser and microwave field manipulation of the atomic states, these interactions form the basis for many quantum information processing schemes [4], including quantum gates with individual atoms [2, 6–9] and atomic ensembles [3, 4, 10]. Furthermore, cold atoms excited to Rydberg states represent a flexible platform to simulate [11] and study few-body [12–21] and many-body physics [22–39].

A paradigmatic interaction phenomenon is the formation of a bound pair of particles. An electron on a large Rydberg orbit scattering off a nearby ground-state atom can weakly bind two atoms into a molecule with permanent dipole moment [12, 13]. Macrodimers of two Rydberg atoms can form due to weak van der Waals (vdW) interactions in an applied static electric field [14, 15] or through strong mixing of orbital angular momentum states [16]. Another binding mechanism relies on the Stark-shifted dipole-dipole (DD) interactions which can support Rydberg dimers [17] and trimers [18].

Here we identify a new mechanism to obtain long-range binding potentials between Rydberg atoms. Our two-atom potential curves result from microwave field coupling between a pair of Rydberg states of each atom [19]. Atoms in these states interact with each other via repulsive and attractive vdW potentials. In addition, there is in general a weaker DD exchange interaction between the atoms on the allowed microwave transition. We find that when the attractive vdW interaction is comparable to, or stronger than, the repulsive vdW (and DD) interaction, the microwave-dressed potential energy curves have pronounced wells. These two-atom binding potentials are located in the vicinity of crossings of the attractive and repulsive potential curves, in the frame rotating with the microwave frequency. The microwave field, which is de-

tuned from the transition resonance of a single atom, lifts the degeneracy and causes level anti-crossing in the two atom basis. We note that the combination of resonant and non-resonant DD interactions between the Rydberg atoms can also result in a binding potential but at a smaller interatomic distance [17].

We next address the question of how to selectively populate these Rydberg-dimer states starting from the two-atom ground state. The strong microwave field induces a broad dark resonance [40] for the laser excitation of a single (non-interacting) atom. We show that within this electromagnetically induced transparency (EIT) [41] window, a smooth probe laser pulse populates only the two-atom Rydberg manifold. We then propose to employ such a Rydberg dimer state to realize high-fidelity quantum logic gate between a pair of qubits represented by atoms trapped at a suitable distance from each other. This is implemented by coherent excitation and de-excitation of the atoms with the probe pulse of an effective area of 2π . The quantum interference responsible for EIT prevents Rydberg excitation of a single atom, and only an appropriate two-atom state acquires a conditional phase π corresponding to the universal CPHASE gate. Since during the gate operation we populate the two-atom Rydberg state at the bottom of a potential well, there is no mechanical force between the atoms and motional decoherence [21] is suppressed.

Consider a pair of atoms with the Rydberg states $|e\rangle$ and $|r\rangle$ coupled by a microwave field with the Rabi frequency Ω and detuning Δ , see Fig. 1(a). In the frame rotating with the microwave field frequency, the interaction Hamiltonian for atom $j = 1, 2$ reads $\mathcal{V}^j = -\hbar\Delta\hat{\sigma}_{rr}^j - \hbar\Omega(\hat{\sigma}_{re}^j + \hat{\sigma}_{er}^j)$, where $\hat{\sigma}_{\alpha\beta}^j \equiv |\alpha_j\rangle\langle\beta_j|$ denote the atomic operators. Atoms in states $|e\rangle$ and $|r\rangle$ interact via the vdW potentials $\mathcal{W}_{ee} = \hbar\hat{\sigma}_{ee}^1\frac{C_6^{ee}}{R^6}\hat{\sigma}_{ee}^2$ and $\mathcal{W}_{rr} = \hbar\hat{\sigma}_{rr}^1\frac{C_6^{rr}}{R^6}\hat{\sigma}_{rr}^2$, where R is the interatomic distance and C_6^{ee} and C_6^{rr} are the corresponding vdW coefficients. There is also a resonant DD (exchange) interaction between the atoms $\mathcal{D}_{er} = \hbar\sum_{i\neq j}\hat{\sigma}_{re}^i\frac{C_3^{er}}{R^3}\hat{\sigma}_{er}^j$, and an effective vdW

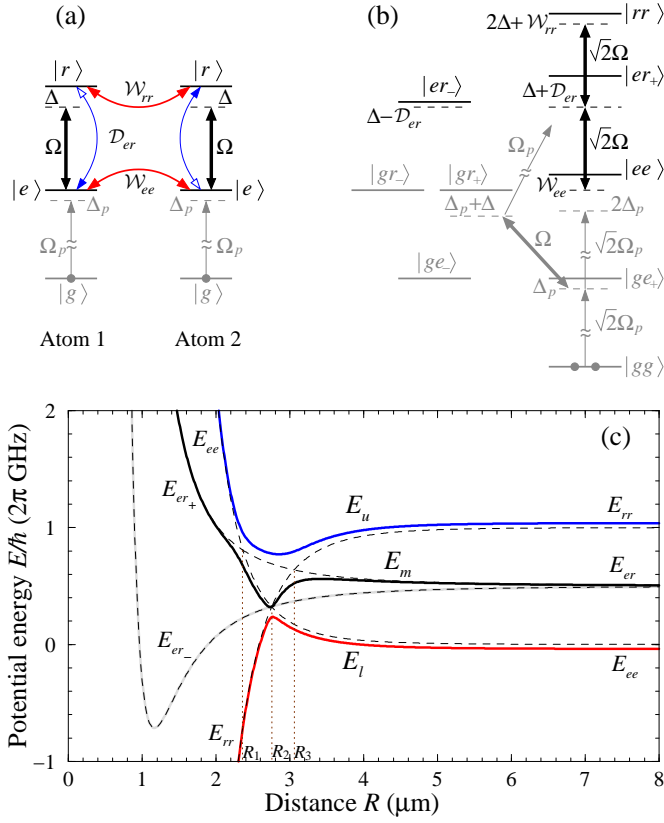


FIG. 1. (a) Atoms 1 and 2 with Rydberg states $|e\rangle$ and $|r\rangle$ interact via repulsive \mathcal{W}_{ee} and attractive \mathcal{W}_{rr} vdW interactions and DD (exchange) interaction \mathcal{D}_{er} , while a microwave field drives the transition $|e\rangle \leftrightarrow |r\rangle$ with Rabi frequency Ω and detuning Δ . The Rydberg states can be excited from the ground state $|g\rangle$ by a probe laser field with the Rabi frequency Ω_p and detuning Δ_p . (b) Diagram of levels and couplings in the two-atom basis. Antisymmetric states $|ge_-\rangle$, $|gr_-\rangle$ and $|er_-\rangle$ are decoupled from the laser and microwave fields. (c) Potential curves E_l , E_m and E_u for the two-atom microwave-dressed Rydberg states of Rb atoms, for $|e\rangle \equiv |60S_{1/2}, m_j = +\frac{1}{2}\rangle$, $|r\rangle \equiv |60P_{3/2}, m_j = +\frac{3}{2}\rangle$ (quantization axis is perpendicular to the two-atom separation vector, see [42]), $\Omega = 2\pi \times 0.1\text{GHz}$ and $\Delta = -5\Omega$. Dashed curves correspond to the bare ($\Omega \rightarrow 0$) energy levels E_{ee} , E_{er_\pm} and E_{rr} crossing at $R_{1,2,3}$.

interaction $\mathcal{W}_{er} = \hbar \sum_{i \neq j} \hat{\sigma}_{rr}^i \frac{C_6^{er}}{R^6} \hat{\sigma}_{ee}^j$ which arises from nonresonant DD interaction with shifted Rydberg level(s) [42]. These DD interactions play a secondary role in our analysis, but we include them for completeness and in order to contrast our results with those of Ref. [17]. The total Hamiltonian for the pair of Rydberg atoms is then given by $\mathcal{H}_{2\text{Ry}} = \mathcal{V}^1 + \mathcal{V}^2 + \mathcal{W}_{ee} + \mathcal{W}_{rr} + \mathcal{D}_{er} + \mathcal{W}_{er}$. Below we focus on the case of a large detuning $|\Delta| \gg \Omega$, as it exhibits rich structure and deep potential wells. The (near-)resonant case $|\Delta| \lesssim \Omega$ is discussed in [42].

Our two-atom basis set consists of states $|ee\rangle \equiv |e_1e_2\rangle$, $|er_\pm\rangle \equiv \frac{1}{\sqrt{2}}(|e_1r_2\rangle \pm |r_1e_2\rangle)$ and $|rr\rangle \equiv |r_1r_2\rangle$, see Fig. 1(b). When $\Omega \rightarrow 0$, the (bare) energies of states $|ee\rangle$ and $|rr\rangle$ are given by $E_{ee}/\hbar = C_6^{ee}/R^6$ and $E_{rr}/\hbar =$

$-2\Delta + C_6^{rr}/R^6$, with $C_6^{ee} > 0$ (repulsive vdW interaction) and $C_6^{rr} < 0$ (attractive vdW interaction) while $\Delta < 0$ (red detuning). In turn, the resonant DD interaction lifts the degeneracy of states $|er_\pm\rangle$ whose energies are $E_{er_\pm}/\hbar = -\Delta \pm C_3^{er}/R^3 + C_6^{er}/R^6$, where the last term, with $C_6^{er} > 0$, is due to the effective vdW interaction [42]. The dependence of bare energy levels $E_{\alpha\beta}$ on R is shown in Fig. 1(c). For vanishing vdW and DD interactions, $R \rightarrow \infty$, $E_{ee} < E_{er_\pm} < E_{rr}$, while in the opposite limit of very strong (compared to $|\Delta|$) interactions, $R \rightarrow 0$, $E_{ee} > E_{er_+} > E_{er_-} > E_{rr}$ (in the rotating frame). There are three level crossing points of interest: $E_{ee} = E_{er_+} \equiv E_{c1}$ at R_1 , $E_{ee} = E_{rr} \equiv E_{c2}$ at R_2 , and $E_{rr} = E_{er_+} \equiv E_{c3}$ at R_3 , see [42].

Consider first the antisymmetric state $|er_-\rangle$. At large distance, the potential $E_{er_-} \propto -R^{-3}$ is attractive due to the long-range resonant DD interaction, but at smaller distances, the repulsive vdW interaction dominates, $E_{er_-} \propto R^{-6}$. Hence, E_{er_-} has a potential well, $\partial_R E_{er_-} = 0$, around $R_- = \sqrt[3]{2C_6^{er}/C_3^{er}}$ where the vdW repulsion overcomes the DD attraction, see Fig. 1(c). This result follows from our simplified treatment of the non-resonant DD interaction as a second-order perturbation, which reduces to an effective vdW interaction \mathcal{W}_{er} , but it captures the essential physics of the binding potential for DD interacting atoms presented in [17]. The antisymmetric state $|er_-\rangle$ will not play a role in our subsequent analysis since it is decoupled from the microwave field, even when $\Omega \neq 0$.

We are thus left with three basis states $|ee\rangle$, $|er_+\rangle$ and $|rr\rangle$ coupled sequentially by the microwave field with the rate $\sqrt{2}\Omega$, see Fig. 1(b). At large distances $R > R_{2,3}$, the vdW (and DD) interactions are much weaker than $|\Delta|$ and the red-detuned ($\Delta < 0$) microwave field induces ac Stark shifts $\pm \frac{2|\Omega|^2}{\Delta}$ of levels $|ee\rangle$ and $|rr\rangle$, see Fig. 1(c). At small distances, $R < R_{1,2}$, the vdW and DD shifts are so large that levels $|ee\rangle$, $|rr\rangle$ and $|er_+\rangle$ decouple from the field. At the bare energy level crossing points R_1 and R_3 , the microwave field becomes resonant with the transitions $|er_+\rangle \leftrightarrow |ee\rangle$ and $|er_+\rangle \leftrightarrow |rr\rangle$. This leads to avoided crossings of the microwave-dressed energy levels E_u and E_m which are repelled from $E_{c1,c3}$ by $\pm\sqrt{2}\Omega$. The upper potential curve E_u has now a broad well near the crossing point R_3 of the bare levels E_{er_+} and E_{rr} determined by the weakly repulsive DD interaction and strongly attractive vdW interaction. For the parameters used in Fig. 1(c), at the bottom of the potential well the vibration frequency of the two-atom relative motion is $\nu_u \simeq 2\pi \times 450\text{kHz}$; see [42] for details of calculation.

Similarly, at the bare level crossing point R_2 , the microwave field couples states $|ee\rangle \leftrightarrow |rr\rangle$, via nonresonant intermediate state $|er_+\rangle$, with the two-photon Rabi frequency $\Omega^{(2)} = \hbar \frac{|\sqrt{2}\Omega|^2}{E_{c2} - E_{er_+}(R_2)}$. Now the microwave-dressed energy levels E_l and E_m are repelled from E_{c2} by $\pm\Omega^{(2)}$, with the result that the middle potential curve

E_m has a narrow well with the minimum near E_{c2} . With the above parameters, $\Omega^{(2)} = 2\pi \times 55$ MHz and the two-atom relative vibrational frequency in the vicinity of the potential well minimum R_m is $\nu_m \simeq 2\pi \times 2$ MHz [42].

We next consider the excitation of the Rydberg states of atoms from the ground state $|g\rangle$ by a laser field acting on the transition $|g\rangle \rightarrow |e\rangle$ with a time-dependent Rabi frequency $\Omega_p(t)$ and variable detuning Δ_p , see Fig. 1(a). This process is described by the interaction Hamiltonian $\mathcal{V}_p^j = \hbar\Delta_p\hat{\sigma}_{gg}^j - \hbar\Omega_p(\hat{\sigma}_{eg}^j + \hat{\sigma}_{ge}^j)$. The total Hamiltonian for the pair of atoms is now $\mathcal{H} = \mathcal{H}_{2\text{Ry}} + \mathcal{V}_p^1 + \mathcal{V}_p^2$. We simulate the dynamics of the system using the master equation for its density operator $\hat{\rho}$, $\partial_t\hat{\rho} = -\frac{i}{\hbar}[\mathcal{H}, \hat{\rho}] + \mathcal{L}\hat{\rho}$, where the Liouvillian $\mathcal{L}\hat{\rho} = \sum_{j=1,2}(\mathcal{L}_g^j\hat{\rho} + \mathcal{L}_e^j\hat{\rho} + \mathcal{L}_r^j\hat{\rho})$, with $\mathcal{L}_\alpha^j\hat{\rho} = \frac{1}{2}[2\hat{L}_\alpha^j\hat{\rho}\hat{L}_\alpha^{j\dagger} - \{\hat{L}_\alpha^{j\dagger}\hat{L}_\alpha^j, \hat{\rho}\}]$, accounts for the relaxation processes affecting the atoms [43, 44]. These include the slow population decay of Rydberg states $|e\rangle, |r\rangle$ with rates $\Gamma_{e,r}$, and the usually more rapid decay of atomic coherences $\hat{\sigma}_{eg}$ and $\hat{\sigma}_{rg}$ with the total rate $\gamma = \gamma_g + \frac{1}{2}\Gamma_{e,r}$ ($\gamma_g \gg \Gamma_{e,r}$) which originates from the laser phase fluctuations, Doppler shifts due to thermal atomic motion, and intermediate state decay when $|g\rangle \rightarrow |e\rangle$ is a two-photon transition [6–8, 10, 38, 39]. The corresponding Lindblad generators are given by $L_e^j = \sqrt{\Gamma_e}\hat{\sigma}_{ge}^j$, $L_r^j = \sqrt{\Gamma_r}\hat{\sigma}_{gr}^j$ and $L_g^j = \sqrt{\gamma_g/2}(\hat{\sigma}_{gg}^j - \hat{\sigma}_{ee}^j - \hat{\sigma}_{rr}^j)$.

We assume that a short probe laser pulse $\Omega_p(t)$ irradiates the pair of atoms, followed by the detection of atoms in the Rydberg states, e.g., through dc field ionization. We vary the probe field frequency Δ_p and interatomic distance R from pulse to pulse to obtain the Rydberg excitation probabilities shown in Fig. 2. The probabilities of a single $P_{1\text{Ry}} = \text{tr}(\hat{\rho}\hat{\Pi}_{1\text{Ry}})$ and double $P_{2\text{Ry}} = \text{tr}(\hat{\rho}\hat{\Pi}_{2\text{Ry}})$ excitations are defined through the projectors $\hat{\Pi}_{1\text{Ry}} \equiv \sum_{i \neq j}(\hat{\sigma}_{ee}^i + \hat{\sigma}_{rr}^i)\hat{\sigma}_{gg}^j$ and $\hat{\Pi}_{2\text{Ry}} \equiv (\hat{\sigma}_{ee}^1 + \hat{\sigma}_{rr}^1)(\hat{\sigma}_{ee}^2 + \hat{\sigma}_{rr}^2)$, where $\hat{\sigma}_{gg}^j + \hat{\sigma}_{ee}^j + \hat{\sigma}_{rr}^j = \mathbf{1}_j$; an actual experiment may or may not resolve the Rydberg state and atom (or ion) number, therefore both $P_{1\text{Ry}}$ and $P_{2\text{Ry}}$ are treated on equal footing.

Clearly, single atom excitation $P_{1\text{Ry}}$, or pair excitation $P_{2\text{Ry}}$ at large interatomic distances R , are unaffected by the Rydberg-state interactions. Scanning the frequency of the laser field, we then probe the microwave field induced Autler-Townes doublet $\lambda_{\pm} = -\frac{1}{2}\Delta \pm \sqrt{\frac{1}{4}\Delta^2 + \Omega^2}$ of the Rydberg states $|e\rangle$ and $|r\rangle$. For large microwave detuning $|\Delta| \gg \Omega$, the probe field resonances are at $\Delta_p^{(-)} = \lambda_- \simeq -\frac{\Omega^2}{|\Delta|}$ and $\Delta_p^{(+)} = \lambda_+ \simeq |\Delta| + \frac{\Omega^2}{|\Delta|}$, as expected [cf. Fig. 1(c)]. Importantly, in the frequency region between $\Delta_p^{(-)}$ and $\Delta_p^{(+)}$, destructive quantum interference leads to a dark resonance (EIT window) for the probe pulse [40, 41]: If the pulse envelope varies adiabatically, $\partial_t\Omega_p < \Omega_p|\lambda_+ - \lambda_-|$, it does not excite the bright eigenstates of the three-level atom, which correspond to the Autler-Townes doublet when $\Omega_p \ll \Omega$. During the interaction with the pulse, the populations of the Ry-

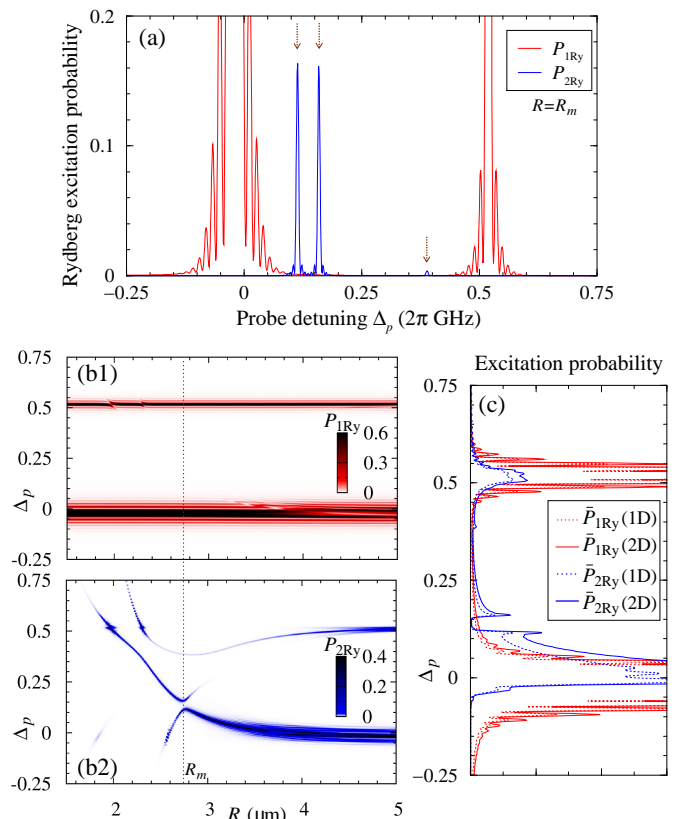


FIG. 2. Rydberg excitation spectra for a pair of atoms excited from the ground state $|gg\rangle$ by a smooth probe pulse $\Omega_p(t)$. (a) One- and two-atom excitation probabilities $P_{1\text{Ry}}$ and $P_{2\text{Ry}}$ at interatomic distance $R_m = 2.74$ μm . (b1), (b2) Density plots of $P_{1\text{Ry}}, P_{2\text{Ry}}$ vs distance R [vertical dotted line marks $R = R_m$, cf. (a)]. (c) Spatially averaged excitation probabilities $\bar{P}_{1\text{Ry}}$ and $\bar{P}_{2\text{Ry}}$ for pairs of atoms in a 1D or 2D volume of linear dimension $L = 5$ μm . In the simulations, the decay rates are $\Gamma_{e,r} = 5$ kHz and $\gamma_g = 2\pi \times 100$ kHz, the probe Rabi frequency $\Omega_p = 2\pi \times 10$ MHz (0.1Ω) and duration $\tau_p = 80$ ns (flat-top pulse with Gaussian leading and trailing edges of 10 ns duration); other parameters are as in Fig. 1(c).

berg states are $\langle\hat{\sigma}_{ee}\rangle \simeq 0$ and $\langle\hat{\sigma}_{rr}\rangle \simeq \frac{\Omega_p^2}{\Omega^2}$, but after the interaction, $\Omega_p \rightarrow 0$, the atom returns to the ground state with ideally unit probability $\langle\hat{\sigma}_{gg}\rangle \simeq 1$. Atomic coherence relaxation γ , however, reduces the transparency causing residual populations of the excited states.

Hence, within the EIT window for a single (non-interacting) atom, we can probe the two-atom Rydberg resonances $E_{l,m,u}$. In Fig. 2(a) we show the Rydberg excitation probabilities versus probe detuning Δ_p for the atoms at distance $R = R_m$ of the E_m potential minimum. Figure 2(b) summarizes the results of our simulations for all (relevant) probe frequencies and interatomic distances. Note that selective excitations of two-atom Rydberg resonances from the ground state, $2\Delta_p = E_{l,m,u}/\hbar$, require two probe photons and such processes are therefore second order in Ω_p , while single-atom resonances

$\Delta_p = \lambda_{\pm}$ involve only one probe photon and are linear in Ω_p . An effective probe Rabi frequency for two-atom excitation is then much smaller than for a single-atom excitation, and in Fig. 2 the smaller peaks of $P_{2\text{Ry}}$ arise from a fractional ($\frac{1}{10}$) two-atom Rabi cycle, while the same amplitude and duration of the probe pulse results in several single-atom Rabi cycles leading to large and broad (sinc-shaped) peaks of $P_{1\text{Ry}}$.

If two atoms are confined in a uniform 1D (line) or 2D (disc) volume of linear dimension L , we can average the Rydberg excitation probabilities over the interatomic distances, $\bar{P}_{1,2\text{Ry}} \equiv \int_0^L P_{1,2\text{Ry}} \varrho(R) dR$, where the corresponding probability densities for distances R are given by $\varrho_{1\text{D}}(R) = \frac{2(L-R)}{L^2}$ and $\varrho_{2\text{D}}(R) = \frac{8R}{\pi L^2} \left[2 \arccos \frac{R}{L} - \frac{R}{2L} \sqrt{1 - \frac{R^2}{L^2}} \right]$. As seen in Fig. 2(c), even after averaging over a large volume, we can still discern the structure of the two-atom Rydberg excitation probabilities $\bar{P}_{2\text{Ry}}$ exhibiting an energy gap $2\Omega^{(2)} \simeq 2\pi \times 0.1\text{GHz}$ between $\max E_l/2\hbar < \Delta_p < \min E_m/2\hbar$, not masked by the single-atom excitation probability $\bar{P}_{1\text{Ry}}$ within the EIT window. Such features may still persist in low-density many-atom experiments, but they will be altered if the probability of having three- or more atoms within a few μm distance from each other becomes comparable to the two-atom probability.

We now describe a potential application of the coherent, selective excitation of the bound Rydberg-dimer state for quantum information processing. Assume that a pair of cold atoms 1 and 2 are trapped at a relative distance $R_0 \simeq R_m$ in an optical lattice [38, 39] or by far-detuned focused laser beams [6–8]. In each atom, long-lived states $\{|s\rangle, |g\rangle\}$ represent the qubit basis states. The probe field resonantly couples the two-atom ground state $|g_1g_2\rangle$ to the bound Rydberg-dimer state with the effective two-photon Rabi frequency $\Omega_p^{(2)} \sim f\Omega_p^2/\Delta_p$, where f is the Franck-Condon overlap between the corresponding relative-coordinate wavefunctions [42]. Atoms in state $|s\rangle$ are decoupled from the field, while single-atom Rydberg excitations from $|g\rangle$ in $|s_1g_2\rangle$ and $|g_1s_2\rangle$ are suppressed by the EIT mechanism. A pulse of effective area $\theta_p = 2 \int_0^\tau \Omega_p^{(2)}(t) dt = 2\pi$ thus leads to precisely one Rabi cycle between $|g_1g_2\rangle$ and the Rydberg-dimer state, while all other initial states remain unaltered. The resulting π phase shift of $|g_1g_2\rangle$ corresponds to the universal two-qubit CPHASE logic gate [43, 44].

We have performed simulations of the two-atom gate using realistic experimental parameters [42]. As seen in Fig. 3(insets), sizable dephasing γ detrimentally affects the amplitude of Rabi oscillations between the two-atom ground and bound Rydberg-dimer states, reducing the final population $P_{gg} = \langle \hat{\sigma}_{gg}^1 \hat{\sigma}_{gg}^2 \rangle$ of state $|g_1g_2\rangle$. To quantify the performance of the gate, we apply it to the initial two-atom state $|\Psi_{\text{in}}\rangle = \frac{1}{2}(|s_1\rangle + |g_1\rangle)(|s_2\rangle + |g_2\rangle)$ containing equally weighted superposition of all two-qubit

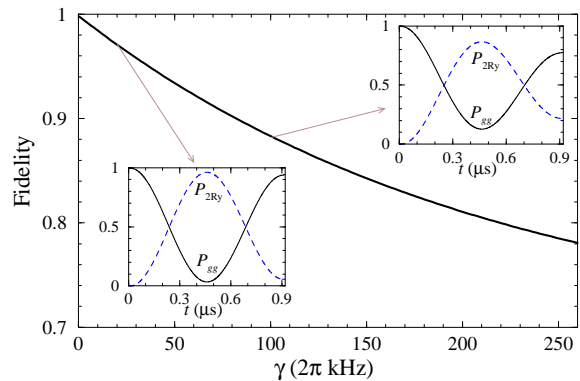


FIG. 3. Fidelity F of CPHASE gate performed on atomic qubits trapped at relative distance R_m vs the dephasing rate γ . Insets show the probabilities P_{gg} and $P_{2\text{Ry}}$ of two-atom ground and bound Rydberg-dimer states during one Rabi cycle, for $\gamma/(2\pi) = 20$ and 100kHz . The probe pulse detuning is $\Delta_p = 2\pi \times 159.3\text{MHz}$, duration $\tau = 0.9\mu\text{s}$ and its single-atom Rabi frequency $\sqrt{f}\Omega_p$ is scaled by the Franck-Condon factor $f = 0.65$ [42]. Other parameters are as in Fig. 2(a).

states. Ideally, the output state should be $|\Psi_{\text{out}}\rangle = \frac{1}{2}(|s_1s_2\rangle + |s_1g_2\rangle + |g_1s_2\rangle - |g_1g_2\rangle)$. In Fig. 3 we show the resulting gate fidelity $F = \langle \Psi_{\text{out}} | \hat{\rho}(\tau) | \Psi_{\text{out}} \rangle$ which is close to unity for small $\gamma \ll \Omega_p^{(2)}$, and decreases with increasing γ due to residual population of Rydberg states at the end of the gate.

Our quantum logic gate implementation complements previous proposals [4] in several ways. For moderate interatomic separation of a few micrometers, the strong interactions are typically used for the blockade gate [2] involving resonant Rydberg excitation of only one atom [6–8], while at larger separation, both atoms can be excited and the interaction then results in a phase shift accumulated over time [2, 9]. One can attempt to excite resonantly an anti-blockaded pair of strongly interacting atoms while suppressing single-atom excitation by large detuning (equal to half of the interaction energy), but then the gradient of the vdW potential will induce a strong mechanical force between the atoms, causing motional decoherence and even excitation suppression [21]. In our implementation of the fast interaction gate, single atom excitations are not merely suppressed by large detuning, but are almost completely canceled by destructive quantum interference, and the gate is much less vulnerable to motional decoherence since we resonantly populate the two-atom bound state at a potential minimum. An additional weak trapping potential for the Rydberg state atoms [4] can compensate the dispersion of the center-of-mass wavefunction of the two atoms [42], insuring their complete return to the trapped ground state.

To conclude, we have shown that an appropriately tuned microwave field can induce deep binding potentials between pairs of strongly-interacting Rydberg atoms. The two-atom Rydberg states can be selectively pop-

ulated from the atomic ground states by smooth laser pulses which concurrently are decoupled from single-atom Rydberg states due to a broad, dark (EIT) resonance affected by the same microwave field. A two-qubit interaction gate can be realized with high-fidelity via the bound Rydberg-dimer state without inducing mechanical forces between the atoms.

We are grateful to I. Lesanovsky and W. Li for valuable input and discussions, and we acknowledge support from the FET-Open grant MALICIA (265522).

-
- [1] T.F. Gallagher, *Rydberg Atoms* (Cambridge University Press, Cambridge, 1994).
- [2] D. Jaksch, J.I. Cirac, P. Zoller, S.L. Rolston, R. Cote, and M.D. Lukin, Phys. Rev. Lett. **85**, 2208 (2000).
- [3] M.D. Lukin, M. Fleischhauer, R. Côté, L.M. Duan, D. Jaksch, J.I. Cirac, and P. Zoller, Phys. Rev. Lett. **87**, 037901 (2001).
- [4] M. Saffman, T.G. Walker, and K. Mølmer, Rev. Mod. Phys. **82**, 2313 (2010).
- [5] D. Comparat and P. Pillet, J. Opt. Soc. Am. B **27**, A208 (2010).
- [6] A. Gaëtan, Y. Miroshnychenko, T. Wilk, A. Chotia, M. Viteau, D. Comparat, P. Pillet, A. Browaeys, and P. Grangier, Nature Phys. **5**, 115 (2009); T. Wilk, A. Gaëtan, C. Evellin, J. Wolters, Y. Miroshnychenko, P. Grangier, and A. Browaeys, Phys. Rev. Lett. **104**, 010502 (2010).
- [7] E. Urban, T.A. Johnson, T. Henage, L. Isenhower, D.D. Yavuz, T.G. Walker, and M. Saffman, Nature Phys. **5**, 110 (2009); L. Isenhower, E. Urban, X. L. Zhang, A. T. Gill, T. Henage, T. A. Johnson, T. G. Walker, and M. Saffman, Phys. Rev. Lett. **104**, 010503 (2010).
- [8] L. Beguin, A. Vernier, R. Chicireanu, T. Lahaye, and A. Browaeys, Phys. Rev. Lett. **110**, 263201 (2013).
- [9] D. D. Bhaktavatsala Rao and K. Mølmer, Phys. Rev. A **89**, 030301(R) (2014).
- [10] Y.O. Dudin, L. Li, F. Bariani, and A. Kuzmich, Nature Phys. **8**, 790 (2012); L. Li, Y.O. Dudin, and A. Kuzmich, Nature **498**, 466 (2013).
- [11] H. Weimer, M. Müller, I. Lesanovsky, P. Zoller, and H.P. Büchler, Nature Phys. **6**, 382 (2010).
- [12] C.H. Greene, A.S. Dickinson, and H.R. Sadeghpour, Phys. Rev. Lett. **85**, 2458 (2000).
- [13] V. Bendkowsky, B. Butscher, J. Nipper, J.P. Shaffer, R. Löw, and T. Pfau, Nature **458**, 1005 (2009); W. Li, T. Pohl, J.M. Rost, S.T. Rittenhouse, H.R. Sadeghpour, J. Nipper, B. Butscher, J.B. Balewski, V. Bendkowsky, R. Löw, and T. Pfau, Science **334**, 1110 (2011).
- [14] C. Boisseau, I. Simbotin, and R. Cote, Phys. Rev. Lett. **88**, 133004 (2002).
- [15] A. Schwettmann, K.R. Overstreet, J. Tallant, and J.P. Shaffer, J. Mod. Opt. **54**, 2551 (2007); K.R. Overstreet, A. Schwettmann, J. Tallant, D. Booth, and J.P. Shaffer, Nature Phys. **5**, 581 (2009).
- [16] N. Samboy, J. Stanojevic, and R. Cote, Phys. Rev. A **83**, 050501(R) (2011).
- [17] M. Kiffner, H. Park, W. Li, and T.F. Gallagher, Phys. Rev. A **86**, 031401(R) (2012).
- [18] M. Kiffner, W. Li, and D. Jaksch, Phys. Rev. Lett. **111**, 233003 (2013).
- [19] Y. Yu, H. Park, and T. F. Gallagher, Phys. Rev. Lett. **111**, 173001 (2013).
- [20] C. Ates, B. Olmos, W. Li, and I. Lesanovsky, Phys. Rev. Lett. **109**, 233003 (2012).
- [21] W. Li, C. Ates, and I. Lesanovsky, Phys. Rev. Lett. **110**, 213005 (2013).
- [22] G. Pupillo, A. Micheli, M. Boninsegni, I. Lesanovsky, and P. Zoller, Phys. Rev. Lett. **104**, 223002 (2010).
- [23] H. Weimer, R. Löw, T. Pfau, and H.P. Büchler, Phys. Rev. Lett. **101**, 250601 (2008).
- [24] H. Weimer and H.P. Büchler, Phys. Rev. Lett. **105**, 230403 (2010).
- [25] T. Pohl, E. Demler, and M.D. Lukin, Phys. Rev. Lett. **104**, 043002 (2010).
- [26] J. Schachenmayer, I. Lesanovsky, A. Micheli, and A.J. Daley, New J. Phys. **12**, 103044 (2010).
- [27] R.M.W. van Bijnen, S. Smit, K.A.H. van Leeuwen, E.J.D. Vredenburg, and S.J.J.M.F. Kokkelmans, J. Phys. B **44**, 184008 (2011).
- [28] I. Lesanovsky, Phys. Rev. Lett. **106**, 025301 (2011).
- [29] I. Lesanovsky, Phys. Rev. Lett. **108**, 105301 (2012).
- [30] W. Zeller, M. Mayle, T. Bonato, G. Reinelt, and P. Schmelcher, Phys. Rev. A **85**, 063603 (2012).
- [31] S. Ji, C. Ates and I. Lesanovsky, Phys. Rev. Lett. **107**, 060406 (2011).
- [32] C. Ates and I. Lesanovsky, Phys. Rev. A **86**, 013408 (2012).
- [33] D. Petrosyan, M. Höning, and M. Fleischhauer, Phys. Rev. A **87**, 053414 (2013).
- [34] M. Höning, D.Muth, D. Petrosyan, and M. Fleischhauer, Phys. Rev. A **86**, 023401 (2013).
- [35] M. Gärttner, K.P. Heeg, T. Gasenzer and J. Evers, Phys. Rev. A **86**, 033422 (2012); Phys. Rev. A **88**, 043410 (2013).
- [36] D. Petrosyan, J. Phys. B **46**, 141001 (2013); Phys. Rev. A **88**, 043431 (2013).
- [37] I. Lesanovsky and J. P. Garrahan Phys. Rev. Lett. **111**, 215305 (2013).
- [38] M. Viteau, M.G. Bason, J. Radogostowicz, N. Malossi, D. Ciampini, O. Morsch, and E. Arimondo, Phys. Rev. Lett. **107**, 060402 (2011).
- [39] P. Schauß, M. Cheneau, M. Endres, T. Fukuhara, S. Hild, A. Omran, T. Pohl, C. Gross, S. Kuhr, and I. Bloch, Nature **491**, 87 (2012).
- [40] K. Bergmann, H. Theuer, and B.W. Shore, Rev. Mod. Phys. **70**, 1003 (1998).
- [41] M. Fleischhauer, A. Imamoglu, and J. P. Marangos, Rev. Mod. Phys. **77**, 633 (2005).
- [42] See Supplemental Material for atomic parameters and interactions, calculations of interatomic potential wells, potential curves for near-resonant microwave field, and excitation of trapped ground state atoms to the Rydberg-dimer state.
- [43] M. Nielsen and I. Chuang, *Quantum Computation and Quantum Information*, (Cambridge University Press, Cambridge, 2000)
- [44] P. Lambropoulos and D. Petrosyan, *Fundamentals of Quantum Optics and Quantum Information*, (Springer, Berlin, 2007).

SUPPLEMENTAL MATERIAL

In these notes, we present details on the Rydberg states of the pair of atoms and their interactions, calculations of interatomic potential wells for large detuning of the microwave field as used in the main text, interatomic potentials for near-resonant microwave field, and the Franck-Condon factor for coherent excitation of trapped ground state atoms to the bound Rydberg dimer state.

Atomic parameters and interatomic interactions

The vector \mathbf{R} connecting the positions of atoms 1 and 2 forms an angle θ with the quantization direction \hat{z} defined by a static electric field \mathbf{E} , see Fig. 4(a). The interaction between the atomic dipoles \wp_1 and \wp_2 is given by

$$\begin{aligned} \mathcal{D} &= \frac{1}{4\pi\epsilon_0} \left[\frac{\wp_1 \cdot \wp_2}{R^3} - 3 \frac{(\wp_1 \cdot \mathbf{R})(\wp_2 \cdot \mathbf{R})}{R^5} \right] \\ &= \frac{1}{4\pi\epsilon_0 R^3} \left[\wp_{1+}\wp_{2-} + \wp_{1-}\wp_{2+} + \wp_{1z}\wp_{2z}(1 - 3\cos^2\theta) \right. \\ &\quad \left. - \frac{3}{2}\sin^2\theta(\wp_{1+}\wp_{2+} + \wp_{1+}\wp_{2-} + \wp_{1-}\wp_{2+} + \wp_{1-}\wp_{2-}) \right. \\ &\quad \left. - \frac{3}{\sqrt{2}}\sin\theta\cos\theta(\wp_{1+}\wp_{2z} + \wp_{1-}\wp_{2z} + \wp_{1z}\wp_{2+} + \wp_{1z}\wp_{2-}) \right] \end{aligned}$$

where $R \equiv |\mathbf{R}|$ while $\wp_{\pm,0}$ denotes the dipole matrix element for the atomic transition changing the magnetic quantum number m_j (projection of the total angular momentum J onto \hat{z}) by $\Delta m_j = \pm 1, 0$. The interaction is invariant under rotation about the \hat{z} axis.

We assume alkali atoms. The two Rydberg states of each atom are represented by $|e\rangle \equiv |nS_{1/2}, m_j = +\frac{1}{2}\rangle$ and $|r\rangle \equiv |nP_{3/2}, m_j = +\frac{3}{2}\rangle$ with the principal quantum number n ($\gtrsim 40$), see Fig. 4(b). A σ_+ -polarized microwave field \mathcal{E}_{mw} of frequency ω_{mw} drives the transition

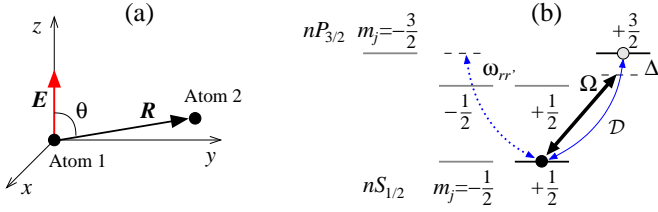


FIG. 4. (a) Geometry of the system of two Rydberg atoms: θ is the angle between the relative position vector \mathbf{R} and the quantization axis z defined by a static external field \mathbf{E} . (b) Level scheme of the magnetic sublevels m_j of states $nS_{1/2}$ and $nP_{3/2}$ of each atom. The microwave field drives the transition between $|e\rangle \equiv |nS_{1/2}, m_j = \frac{1}{2}\rangle$ and $|r\rangle \equiv |nP_{3/2}, m_j = \frac{3}{2}\rangle$ with the Rabi frequency Ω and detuning Δ . Resonant DD (exchange) interaction \mathcal{D} can swap the states $|e_1\rangle|r_2\rangle \leftrightarrow |r_1\rangle|e_2\rangle$ of the two atoms, while the transition to $|r'\rangle \equiv |nP_{3/2}, m_j = -\frac{1}{2}\rangle$ is non-resonant due to the \mathbf{E} field induced differential Stark shift $\omega_{rr'}$.

$|e\rangle \leftrightarrow |r\rangle$ with the Rabi frequency $\Omega = \wp_{er}\mathcal{E}_{\text{mw}}/\hbar$ and detuning $\Delta = \omega_{\text{mw}} - \omega_{re}$. For $\theta = \frac{\pi}{2}$, the DD interaction reduces to

$$\mathcal{D} = -\frac{\wp_{1+}\wp_{2-} + \wp_{1-}\wp_{2+}}{8\pi\epsilon_0 R^3} - 3\frac{\wp_{1+}\wp_{2+} + \wp_{1-}\wp_{2-}}{8\pi\epsilon_0 R^3}. \quad (1)$$

Here the first term on the right-hand side describes the resonant exchange interaction $|e_{1(2)}r_{2(1)}\rangle \leftrightarrow |r_{1(2)}e_{2(1)}\rangle$ denoted by \mathcal{D}_{eg} in the main text. The transition matrix elements are $\wp_{\pm} = \mp \frac{1}{\sqrt{3}}(nS_{1/2}||\wp||nP_{3/2})$, where the numerical prefactor corresponds the angular part while the reduced matrix element in the semiclassical approximation [1] is given by $(nS_{1/2}||\wp||nP_{3/2}) \approx -\frac{3}{2}n^{*2}$ with $n^* = n - \delta_S$ the effective principal quantum number. The DD coefficient is then $C_3^{er} \approx \frac{3n^{*4}}{32\pi\epsilon_0}$. The second term on the right-hand side of Eq. (1) corresponds to the DD interaction coupling states $|e_{1(2)}r_{2(1)}\rangle$ to $|r'_{1(2)}e_{2(1)}\rangle$ with the rate $C_3^{er,r'e} \approx \frac{3\sqrt{3}n^{*4}}{32\pi\epsilon_0}$. This process could populate the state $|r'\rangle \equiv |nP_{3/2}, m_j = -\frac{1}{2}\rangle$ outside the two-level subspace $\{|e\rangle, |r\rangle\}$, but we assume that this leakage is suppressed by the external electric \mathbf{E} (or magnetic) field inducing differential Stark (or Zeeman) shift $\omega_{rr'}$ between levels $|r\rangle$ and $|r'\rangle$, see Fig. 4(b). The non-resonant DD interaction induces, however, a second-order level shift of states $|e_{1(2)}r_{2(1)}\rangle$, which we account for as an effective vdW interaction $\mathcal{W}_{re} = \hbar\delta_{rr'}^{1(2)}\frac{C_6^{er}}{R^6}\delta_{ee}^{2(1)}$ with the coefficient $C_6^{er} = |C_3^{er,r'e}|^2/\omega_{rr'}$, which is positive (repulsive vdW interaction) if the level $|r'\rangle$ is lower than $|r\rangle$. We note that this is a rather simplistic approximation which, strictly speaking, is valid only at large enough distances $R > \sqrt[3]{|C_3^{er,r'e}|/\omega_{rr'}}$. The combination of resonant and nonresonant DD interactions and the resulting binding potential was analyzed rigorously in [2], while our simplification facilitates derivation of the hitherto unexplored binding potentials originating from microwave dressing of vdW interacting states $|e_1e_2\rangle$ and $|r_1r_2\rangle$.

To be specific, we consider Rb atoms in $n = 60$ states. The quantum defects for the $S_{1/2}$ and $P_{3/2}$ states are $\delta_S = 3.13109$ and $\delta_P = 2.65145$ [3], with which the (unshifted) $|e\rangle \rightarrow |r\rangle$ transition frequency is $\omega_{re} \simeq 2\pi \times 17$ GHz. For the DD interaction, we obtain $C_3^{er} \approx 2\pi \times 3.8\text{GHz}\mu\text{m}^3$ and assume $C_6^{er} = 2\pi \times 3\text{GHz}\mu\text{m}^6$. With $\theta = \frac{\pi}{2}$, the coefficients for the vdW potentials \mathcal{W}_{ee} and \mathcal{W}_{rr} used in the main text are $C_6^{ee} \simeq 2\pi \times 140\text{GHz}\mu\text{m}^6$ (repulsion) and $C_6^{rr} \simeq -2\pi \times 295\text{GHz}\mu\text{m}^6$ (attraction) [4, 5].

Crossing points of $E_{\alpha\beta}$ and potential minima of $E_{m,u}$

For vanishing microwave field amplitude, $\Omega \rightarrow 0$, the crossing points of the bare two-atom potentials E_{ee} ,

E_{er+} , and E_{rr} are

$$E_{ee} = E_{er+} \equiv E_{c1} = \frac{4\hbar\Delta^2 C_6^{ee}}{\left[\sqrt{(C_3^{er})^2 + 4|\Delta|(C_6^{ee} - C_6^{er}) - C_3^{er}}}\right]^2}$$

$$\text{at } R_1 = \left[\sqrt{\left(\frac{C_3^{er}}{2\Delta}\right)^2 + \frac{C_6^{ee} - C_6^{er}}{|\Delta|} - \frac{C_3^{er}}{2|\Delta|}} \right]^{1/3},$$

$$E_{rr} = E_{er+} \equiv E_{c3} = -2\hbar\Delta + \frac{4\hbar\Delta^2 C_6^{rr}}{\left[\sqrt{(C_3^{er})^2 + 4|\Delta|(C_6^{er} - C_6^{rr}) + C_3^{er}}}\right]^2}$$

$$\text{at } R_3 = \left[\sqrt{\left(\frac{C_3^{er}}{2\Delta}\right)^2 + \frac{C_6^{er} - C_6^{rr}}{|\Delta|} + \frac{C_3^{er}}{2|\Delta|}} \right]^{1/3},$$

and

$$E_{ee} = E_{rr} \equiv E_{c2} = \frac{2\hbar|\Delta|C_6^{ee}}{C_6^{ee} - C_6^{rr}} \text{ at } R_2 = \sqrt[6]{\frac{C_6^{ee} - C_6^{rr}}{2|\Delta|}}.$$

With the atomic parameters listed above, we have $R_1 \simeq 2.36 \mu\text{m}$, $R_2 \simeq 2.75 \mu\text{m}$, and $R_3 \simeq 3.05 \mu\text{m}$.

In Fig. 1(c) of the main text, the potential energy curves E_m and E_u have potential minima. Consider first the potential well on the E_m curve which is defined by the bare energy levels E_{ee} and E_{rr} crossing at R_2 . The microwave field couples states $|ee\rangle$ and $|rr\rangle$ by a two-photon transition via non-resonant intermediate state $|er_+\rangle$ with the effective Rabi frequency $\Omega^{(2)} = \frac{\hbar|\sqrt{2}\Omega|^2}{E_{c2} - E_{er+}}$.

At R_2 , we have $E_{er+} \approx \hbar|\Delta| + \frac{\hbar C_3^{er} \sqrt{2|\Delta|}}{\sqrt{C_6^{ee} - C_6^{rr}}}$, which upon substitution leads to

$$\Omega^{(2)} = \frac{2|\Omega|^2(C_6^{ee} - C_6^{rr})}{|\Delta|(C_6^{ee} + C_6^{rr}) - C_3^{er} \sqrt{2\Delta}(C_6^{ee} - C_6^{rr})}.$$

For our parameters, both terms in the denominator are comparable and hence the DD interaction cannot be neglected. We obtain $|\Omega^{(2)}| \simeq 2\pi \times 55 \text{ MHz}$.

In the vicinity of E_{c2} and R_2 , we thus have an effective two-level system described by Hamiltonian

$$\mathcal{H}_{\text{eff}} = \begin{bmatrix} E_{ee}^{(1)} & \hbar\Omega^{(2)} \\ \hbar\Omega^{(2)} & E_{rr}^{(1)} \end{bmatrix},$$

where $E_{\alpha\alpha}^{(1)} = E_{c2} + \eta_{\alpha\alpha}(R - R_2)$ are linear approximations for the bare energies of the corresponding states ($\alpha\alpha = ee, rr$), with $\eta_{\alpha\alpha} = \frac{\partial E_{\alpha\alpha}}{\partial R}|_{R_2}$. The binding potential is $E_m = \frac{1}{2}[E_{ee}^{(1)} + E_{rr}^{(1)}] + \sqrt{\frac{1}{4}[E_{ee}^{(1)} - E_{rr}^{(1)}]^2 + |\hbar\Omega^{(2)}|^2}$,

whose minimum R_m is found by $\partial_R E_m = 0$. Expanding E_m up to the second order in R around R_m , we have $E_m \approx (E_{c2} + \hbar\Omega^{(2)}) + \frac{1}{2}\kappa_m(R - R_m)^2$ with

$$\kappa_m = \frac{2}{\hbar|\Omega^{(2)}|} \frac{|\eta_{ee}\eta_{rr}|^{3/2}}{|\eta_{ee}| + |\eta_{rr}|} = \frac{2\hbar(12\Delta)^2(C_6^{ee}|C_6^{rr}|)^{3/2}}{R_2^2|\Omega^{(2)}|(C_6^{ee} + |C_6^{rr}|)^3}.$$

Since $\kappa_m = \mu\nu_m^2$, with μ the reduced mass, the relative vibration frequency of two identical atoms of mass M_{at} is

$\nu_m \approx \sqrt{2\kappa_m/M_{\text{at}}}$. With the parameters for ^{87}Rb atoms listed above, we obtain $\nu_m \simeq 2\pi \times 2 \text{ MHz}$ around $R_m = 2.74 \mu\text{m}$.

Consider now the E_u potential energy curve. The potential well is bounded by E_{ee} on the left and E_{rr} on the right sides, and E_{er+} at the bottom. Since with increasing distance R the DD interaction slowly lowers E_{er+} while E_{rr} rapidly approaches $2|\Delta|$, the minimum of the potential well is located above, and to the left from, the energy level crossing point E_{c3} , R_3 of the bare states $|er_+\rangle$ and $|rr\rangle$ coupled by the microwave field with the Rabi frequency $\sqrt{2}\Omega$. Now the Hamiltonian for the effective two-level system is

$$\mathcal{H}_{\text{eff}} = \begin{bmatrix} E_{er+}^{(1)} & \hbar\sqrt{2}\Omega \\ \hbar\sqrt{2}\Omega & E_{rr}^{(1)} \end{bmatrix},$$

where $E_{\alpha\beta}^{(1)} = E_{c3} + \eta_{\alpha\beta}(R - R_3)$ with $\eta_{\alpha\beta} = \frac{\partial E_{\alpha\beta}}{\partial R}|_{R_3}$. Proceeding as above, we obtain for the potential well $E_u \approx (E_{c3} + \hbar\sqrt{2}\Omega) + \frac{1}{2}\kappa_u(R - R_u)^2$ with

$$\kappa_u = \frac{2}{\hbar\sqrt{2}|\Omega|} \frac{|\eta_{er+}\eta_{rr}|^{3/2}}{|\eta_{er+}| + |\eta_{rr}|} \simeq \frac{2\hbar}{R_3^2} \frac{9|\Delta|^{5/4}(C_3^{er})^{3/2}}{|\Omega||C_6^{rr}|^{3/4}},$$

where we assumed $R_3 \simeq \sqrt[6]{|C_6^{rr}/\Delta|}$ and neglected $C_3^{er}R_3^3$ in comparison with $2|C_6^{rr}|$ since the DD interaction varies slowly compared to the vdW interaction. For the vibration frequency of the two-atom relative motion around $R_u = 2.85 \mu\text{m}$, we then obtain $\nu_u \approx 2\pi \times 450 \text{ kHz}$.

Two-atom potentials for near-resonant microwave field

In the main text, we considered the case of a large negative detuning $\Delta < -|\Omega|$ of the microwave field from the single-atom transition resonance $|e\rangle \rightarrow |r\rangle$, which leads to two binding potentials with the depths $\sim |\Delta|$. Here we outline the (near-) resonant case $|\Delta| \lesssim |\Omega|$.

In Fig. 5 (main panel) we show the potential energy curves for $\Delta = 0$ and $\Omega \neq 0$. Consider again the bare two-atom states $|ee\rangle$, $|er_{\pm}\rangle$, and $|rr\rangle$. The antisymmetric state $|er_{-}\rangle$ is decoupled from the field at any relative distance R , so its behavior is the same for any Δ which simply shifts the zero-point energy. At large distances $R > R_b \simeq \sqrt[6]{C_6^{\alpha\beta}/\Omega}$, $\sqrt[3]{C_3^{er}/\Omega}$, all two-atom states $|\alpha\beta\rangle$ have the same energy $E_{\alpha\beta} = 0$ (in the frame rotating with the microwave frequency). The microwave field couples resonantly the transitions $|ee\rangle \leftrightarrow |er_+\rangle$ and $|er_+\rangle \leftrightarrow |rr\rangle$ with the same Rabi frequency $\sqrt{2}\Omega$. The eigenstates of the system are then $|\Psi_0\rangle = \frac{1}{\sqrt{2}}(|ee\rangle - |rr\rangle)$ and $|\Psi_{\pm}\rangle = \frac{1}{2}(|ee\rangle \pm |er_+\rangle + |rr\rangle)$ with the corresponding energies $E_0 = 0$ and $E_{\pm}/\hbar = \pm 2\Omega$, as can be observed in Fig. 5. At small distances $R < R_b$, the vdW (and DD) shifted states $|ee\rangle$ and $|rr\rangle$ (and $|er_+\rangle$) are completely

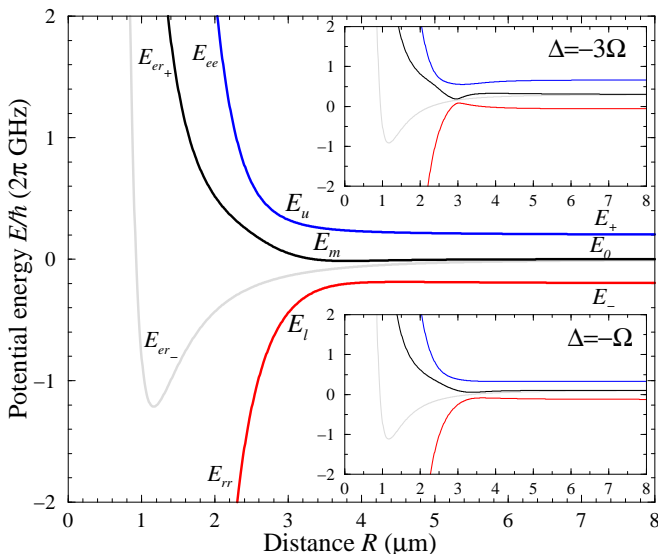


FIG. 5. Potential curves $E_{l,m,u}$ for the two-atom microwave-dressed Rydberg states, for the same parameters as in Fig. 1(c) of the main text, but with $\Delta = 0$ (main panel), and $\Delta = -\Omega$ (lower inset) and $\Delta = -3\Omega$ (upper inset).

decoupled from the microwave field. The transition between the two regimes occurs in the vicinity of $R = R_b$. If the attractive vdW interaction is stronger than the repulsive one, $|C_6^{rrr}| > C_6^{ee}$, there is a shallow potential well on the middle curve E_m (in the opposite case of $|C_6^{rrr}| < C_6^{ee}$ there would be a small hump).

With lowering the frequency of the microwave field to increase the absolute (but negative) value of the detuning $\Delta \sim -|\Omega|$, the potential well on the E_m curve becomes more pronounced [Fig. 5 lower inset]; for still larger (negative) values of $\Delta \lesssim -\Omega$, the potential energy curves approach those described in the main text [Fig. 5 upper inset].

There are no potential wells for positive detuning $\Delta > 0$, if $C_6^{rrr} < 0$ and $C_6^{ee} > 0$. The situation would be reverse for repulsive vdW interaction between the upper Rydberg states $C_6^{rrr} > 0$ and attractive interaction between the lower states $C_6^{ee} < 0$, i.e., we would need $\Delta > 0$ to obtain binding potentials.

Excitation of trapped ground state atoms to the Rydberg-dimer state

We assume that the atoms $j = 1, 2$ in the ground internal state $|g\rangle$ are localized around positions $r_{j,0}$ of two separate traps. For cold atoms, we can approximate the spatial wavefunctions of the atoms ψ_j by the ground-state wavefunction of a harmonic oscillator

$$\psi_j(r_j) \approx \left(\frac{1}{\pi\sigma^2}\right)^{\frac{1}{4}} e^{-\frac{(r_j - r_{j,0})^2}{2\sigma^2}},$$

where the width $\sigma = \sqrt{\hbar/M_{\text{at}}\nu}$ is expressed through the vibrational frequency ν assumed to be the same for both

atoms. The two-atom wavefunction $\Psi_{12} = \psi_1\psi_2$ can be expressed in terms of the center of mass $\bar{r} = \frac{1}{2}(r_1 + r_2)$ and relative $R = r_2 - r_1$ coordinates as $\Psi_{12}(\bar{r}, R) = \phi(\bar{r})\chi(R)$ with

$$\phi(\bar{r}) = \left(\frac{1}{\pi\bar{\sigma}^2}\right)^{\frac{1}{4}} e^{-\frac{(\bar{r}-\bar{r}_0)^2}{2\bar{\sigma}^2}},$$

$$\chi(R) = \left(\frac{1}{\pi\Sigma^2}\right)^{\frac{1}{4}} e^{-\frac{(R-R_0)^2}{2\Sigma^2}},$$

where $\bar{r}_0 = \frac{1}{2}(r_{1,0} + r_{2,0})$ and $R_0 = r_{2,0} - r_{1,0}$, while $\bar{\sigma} = \frac{1}{\sqrt{2}}\sigma$ and $\Sigma = \sqrt{2}\sigma$.

Our aim is to coherently and reversibly excite the two ground state atoms to the Rydberg dimer state on the E_m potential energy curve. We therefore assume an appropriate distance between the trapped atoms $R_0 \simeq R_m$ and apply the probe field Ω_p which is two-photon resonant between the internal-motional ground state $|G\rangle = |g_1g_2\rangle \otimes \chi(R)$ and the Rydberg-dimer state $|D_m\rangle = |\Psi_m\rangle \otimes \chi_m(R)$ with

$$\chi_m(R) = \left(\frac{1}{\pi\Sigma_m^2}\right)^{\frac{1}{4}} e^{-\frac{(R-R_m)^2}{2\Sigma_m^2}},$$

where $\Sigma_m = \sqrt{2\hbar/M_{\text{at}}\nu_m}$. The corresponding Franck-Condon factor for the transition $|G\rangle \rightarrow |D_m\rangle$ is

$$f = \int_0^\infty \chi^*(R)\chi_m(R) dR = \left(\frac{2\Sigma\Sigma_m}{\Sigma^2 + \Sigma_m^2}\right)^{\frac{1}{2}} e^{-\frac{(R_0 - R_m)^2}{2(\Sigma^2 + \Sigma_m^2)}},$$

where we included the contribution of a possible mismatch between the equilibrium interatomic distance R_0 in the ground state traps and the position R_m of the two-atom potential minimum in the Rydberg state. Taking the trap frequency $\nu \simeq 2\pi \times 100$ kHz for the ground-state ^{87}Rb atoms, while for the Rydberg-dimer state we have $\nu_m \simeq 2\pi \times 2$ MHz (see above), we obtain $\Sigma \simeq 48$ nm and $\Sigma_m \simeq 10.7$ nm. Assuming small mismatch $|R_0 - R_m| \ll \Sigma$ leads to the Franck-Condon factor $f \simeq 0.65$ used in Fig. 3 of the main text. Unless we apply a trapping potential for the Rydberg excited atoms, their center-of-mass will disperse freely and a corresponding Franck-Condon factor should be included if the atoms are later driven back to the trapped ground states.

-
- [1] B. Kaulakys, J. Phys. B **28**, 4963 (1995).
 - [2] M. Kiffner, H. Park, W. Li, and T.F. Gallagher, Phys. Rev. A **86**, 031401(R) (2012).
 - [3] T.F. Gallagher, *Rydberg Atoms* (Cambridge University Press, Cambridge, 1994).
 - [4] A. Reinhard, T. Cubel Liebisch, B. Knuffman, and G. Raithel, Phys. Rev. A **75**, 032712 (2007).
 - [5] K. Singer, J. Stanojevic, M. Weidemüller, and R. Côté, J. Phys. B **38**, S295 (2005).